

Experimental geocology

Martynov¹ K.V., Zakharova¹ E.V., Nekrasov² A.N., Kotelnikov² A.R. Influence of cooling rate of the phosphate melt on phase composition and properties of its solidification products

¹A.N. Frumkin Institute of Physical Chemistry and Electrochemistry RAS, Moscow

²Institute of Experimental Mineralogy RAS, Chernogolovka Moscow district

Abstract. It is experimentally proved that at slow cooling of $\text{Na}_2\text{O-Al}_2\text{O}_3\text{-P}_2\text{O}_5$ melt used for a solidification of liquid high level waste (HLW) in glass matrix the glass-crystal product can be formed. In process of fall of temperature in model experiments partial crystallization of melt was followed by differentiation of main glass-forming components and HLW simulators between the coexisting phases: Al, Cr, Fe concentrated in a crystal phase $\text{Na}_7(\text{Al,Cr,Fe})_4(\text{P}_2\text{O}_7)_4\text{PO}_4$; Ca, Ni, La, U collected in the residual melt as a result transformed to glass. Leaching rate of this glass, and together with it, of simulators of radionuclides (La, U) exceeded the expected rate on three orders because of reduction of Al_2O_3 content in the glass in comparison with composition of starting melt. To avoid emergence of negative effects in the course of melt cooling during vitrification of real HLW, two alternative ways are offered.

Key words: vitrification of HLW, melting diagram, crystallization differentiation, leaching rate.

Citation: Martynov, K.V., E.V. Zakharova, A.N. Nekrasov, A.R. Kotelnikov. 2015. Influence of cooling rate of the phosphate melt on phase composition and properties of its solidification products. *Experimental Geochemistry*. Vol. 3. No. 4. P. X-XX.

http://exp-geochem.ru/JPdf/2015/04/Martynov01_eng.pdf

The most dangerous radioactive waste of a nuclear fuel cycle is liquid highly level waste (HLW). The modern conception of treatment of such waste consists in their solidification and isolation

from the biosphere in rocks of earth crust. So far the only industrial technology of liquid HLW solidification in our country is their processing in phosphate glass at PA "Mayak". The composition, structure and properties of phosphate glasses are defined not only by the composition and temperature conditions of melting of furnace mixture, but also by mode of melt cooling [Vashman, 1997]. Really, a cooling rate of a melt is easily regulated in vitro, and for receiving homogeneous glass without crystal inclusions it is tried to support highest rate (a quenching method). At PA "Mayak" spilling of phosphate melt is made at a temperature 850°C from EP-500 ceramic furnace into cans with a capacity of 220 l [Polyakov, 1994]. The valuation by Newton-Rikhman's heat equation shows that after spilling, the central part of a can is cooled from 850 to 450°C approximately during 13 hours with an average rate of 30 grad/hour (fig. 1). Thus, the problem of crystallization of phosphate melts is actual at slow cooling under production conditions, but the composition and structure of the products which are formed thus are a little studied, therefore, there is no convincing explanation of the reasons of change of their physical and chemical properties. It induced us to reproduce melting process of the furnace mixture having the procedural components contents [Polyakov, 1994] including simulators of radionuclides: La and U (tab. 1), with the subsequent slow cooling of the melt, and to study composition and resistance to leaching of the received material.

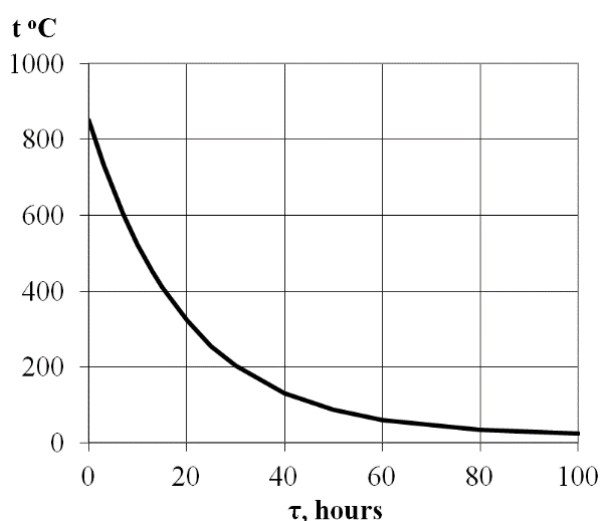


Fig. 1. Cooling rate of phosphate melt containing HLW at PA "Mayak".

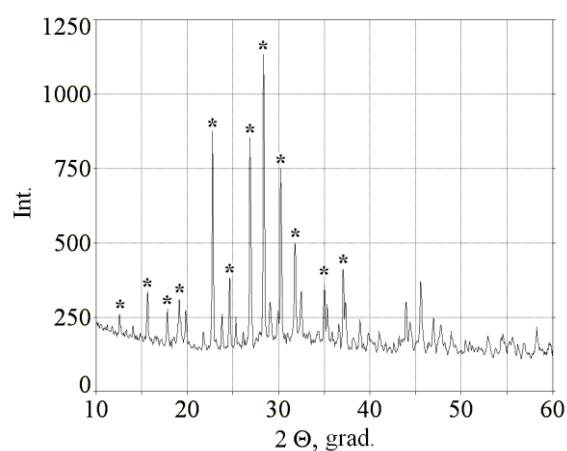


Fig. 2. XRD pattern of experiment products on solidification of model phosphate melt.

Table 1. Chemical composition of the starting mixture and products of phosphate melt solidification, mas. %

Component	Mixture	Glass	Crystal phase	
			Before leaching	After leaching
Na ₂ O	23.7	26±3	20±1	19.4±0.3
Al ₂ O ₃	14.6	3.0±0.9	17±1	16.8±0.4
P ₂ O ₅	54.3	62±2	60±1	61.4±0.2
SO ₃	0.4	0.2±0.1	0.08±0.05	0.08±0.03
CaO	1.4	2.2±0.4	0.6±0.4	0.20±0.06
Cr ₂ O ₃	0.2	0.09±0.01	0.4±0.1	0.3±0.1
Fe ₂ O ₃	1.4	0.1±0.1	1.6±0.3	1.6±0.1
NiO	1.1	1.3±0.4	0.5±0.1	0.31±0.04
La ₂ O ₃	1.6	2.8±0.6	0.2±0.1	0.1±0.1
UO ₃	1.3	2.3±0.7	0.4±0.2	0.05±0.07

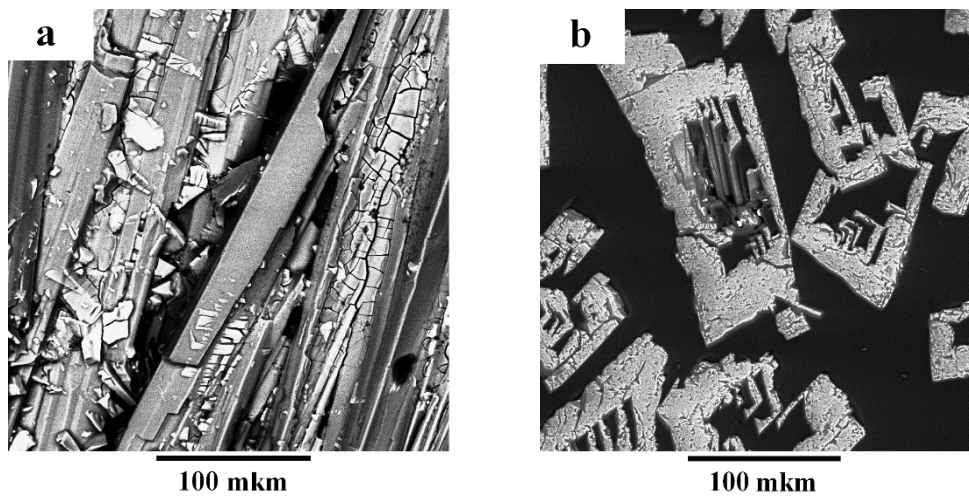


Fig. 3. SEM-images of products of phosphate melt solidification before (a) and after (b) leaching.

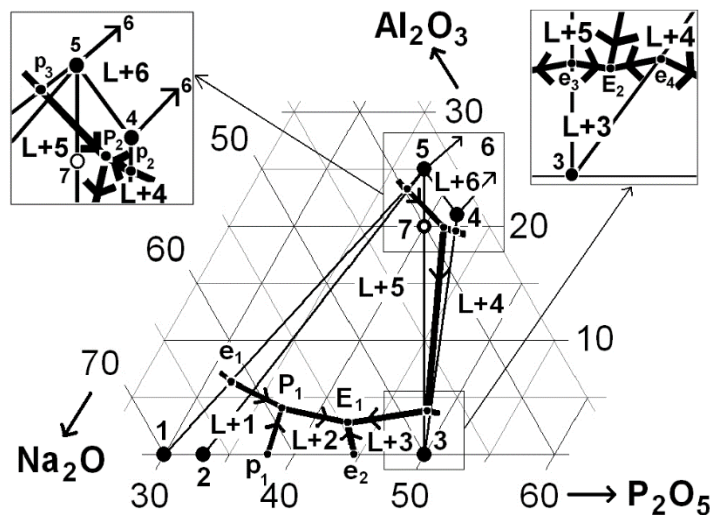


Fig. 4. Topological scheme of the phase diagram of the system Na₂O-Al₂O₃-P₂O₅: E and P – triple (four-phase) invariant eutectic and peritectic points; e and p – double (three-phase) invariant eutectic and peritectic points; L – melt; crystal phases: 1 – Na₄P₂O₇, 2 – Na₅P₃O₁₀, 3 – NaPO₃, 4 – Na₇Al₄(P₂O₇)₄PO₄, 5 – Na₃Al₂(PO₄)₃, 6 – AlPO₄; 7 – procedural composition of the melt; arrows on monovariant lines show the direction of fall of temperature.

The mixture made of solid reagents: NaPO₃, Al(OH)₃, Na₂SO₄, Ca(NO₃)₂·4H₂O, Cr(NO₃)₃·9H₂O, Fe(NO₃)₃·9H₂O, Ni(NO₃)₂·6H₂O, La(NO₃)₃·6H₂O, UO₂(NO₃)₂·6H₂O, was calcinated at a temperature 300°C, grinded in porcelain mortar and melted in corundum (Al₂O₃) crucibles with a diameter of 20 mm in the muffle furnace at gradual fall of temperature from 1000 to 900°C within 5 hours.

After that the furnace was switched off, and the melt cooled down together with the furnace up to 500°C during two hours with an average rate of 200°C/hour. It corresponds to cooling rate of peripheral parts of a can. As a result of keeping of such temperature condition opaque material of green color turned out. It filled ground part of crucibles and had an equal smooth surface with a small meniscus. Thickness of

samples made 2.5-3 mm, weight – 1.5-2 g, calculated density – 2.0 g/cm³. Products of phosphate melt solidification were studied by methods of X-ray diffraction (XRD) and the scanning electronic microscopy (SEM) with electron probe microanalysis (EPMA). Powder XRD patterns were removed at the room temperature on Carl Zeiss URD-63 diffractometer, CuK_α radiation, Ni filter ($\lambda=1.5418$ Å). The microstructure and element compositions of samples were studied on SEM Tescan Vega II XMU with detectors of secondary and backscattered electrons and X-ray energy dispersive Oxford Instruments INCAx-sight spectrometer.

On XRD pattern of experiment products (fig. 2) the reflections of crystal polyphosphate of Na₇Al₄(P₂O₇)₄PO₄ noted by asterisks prevail (PDF-2 #38-0128), and halo from amorphous phase (glass) is visible in area 22-38°2 θ . Polyphase structure of the material consisting from long crystals with an interstitia filled with cracked glass is well visible in electronic microscope (fig. 3a). Elemental composition of crystals according to EPMA results can be expressed by crystal chemical formula Na_{6.97}Al_{3.45}Ca_{0.09}Cr_{0.07}Fe_{0.21}Ni_{0.07}P_{9.11}O₃₂ (tab. 1). As a result of the partial crystallization accompanying melt solidification there was a redistribution of elements between crystal phase and glass: Al, Cr, Fe passed into a crystal phase almost completely; Ca, Ni, La, U and small part of Al remained in the glass which had mainly sodium-phosphate composition. Such differentiation of phases compositions in comparison with initial melt composition, had be reflected inevitably in resistance of polyphase product to leaching. Essential reduction of the content of alumina in glass was especially disturbing, because it causes considerable decrease of phosphate glasses resistance to leaching [Vashman, 1997].

The tendencies of composition changes of phosphate melt in the course of its partial crystallization and of the glass which is formed of residual melt, will become natural and clear if to analyze the melting phase diagram of the system Na₂O-Al₂O₃-P₂O₅. Much to astonishment of, it appeared that after half a century of research of this system and after 30 years of industrial application of technology of HLW immobilization in phosphate glasses, its phase diagram remained not studied. Moreover, possible topological options aren't even analyzed for three-component system, while regional binary sections are investigated experimentally rather well. So one of the last attempts to obtain experimental data in NaPO₃-Al₂O₃ section [Gusarov, 2002] didn't clear up this question because authors couldn't analyze correctly and more exhaustively the results.

Based on known experimental data, we offer the version of melting diagram for area of Na₂O-Al₂O₃-P₂O₅ system surrounding procedural composition of

Mayak's glasses (fig. 4). The main feature of system is incongruent melting of three-component crystal phases: Na₃Al₂(PO₄)₃ and Na₇Al₄(P₂O₇)₄PO₄. The figurative point of procedural composition lies on the Na₃Al₂(PO₄)₃-NaPO₃ line in the area of Na₃Al₂(PO₄)₃ crystallization. Small (less than 3 mol. %) changes of melt composition, quite admissible in conditions of production, can also lead to crystallization of AlPO₄ and Na₇Al₄(P₂O₇)₄PO₄ in different sequences depending on the location of the figurative point in different bivariant fields of the diagram. As a result in process of fall of temperature the equilibrium melt composition will be changed towards E₁ and E₂ eutectics with final crystallization of the readily soluble phases Na₅P₃O₁₀ and NaPO₃. But in actual practice it usually doesn't reach because of increase of melt viscosity with fall of temperature up to formation of glass. However the composition of this glass can be rather strongly displaced concerning the composition of initial melt, as showed our experiments. Besides, for the kinetic reasons at real final association there can be a metastable phase AlPO₄ participating in incomplete peritectic reactions.

Tests on leaching of the synthesized material by distilled water were carried out at a temperature 25°C in a drying box with a temperature regulator in polypropylene hermetic test tubes of 50 ml volume. Thus glass-crystal material wasn't extracted from crucibles, and immersed in test tubes together with them. The area of contact was considered as the geometrical area of an open surface (a little more than 3 cm²). Procedure of tests corresponded to the GOST state standard R52126-2003. The volume of contact solutions made 40 ml. The contact solutions were changed after 1, 3, 7, 15, 28 and 57 days from the beginning of tests. The contents of elements in the leachants were determined by methods of inductively coupled plasma mass spectrometry (Perkin Elmer Elan-6100) and inductively coupled plasma emission spectrometry (Perkin-Elmer Optima-4300 DV). The technique of processing of experimental data was similar used in [Martynov, 2014].

Results of tests are presented in fig. 5 in the form of dependence of integrated leaching rates of material determined by separate elements from the total duration of process. For the first three short intervals of leaching there are shown data based on 10 elements, total is 30 points, for three longer intervals – on 9 elements (except sulfur which wasn't found in the leachants), total is 27 points. After 7 days (vertical dashed line in fig. 5) the leaching rate of material on all elements goes down in steps. With what such dynamics of leaching rate change is connected it was succeeded to understand, having studied material after the end of tests. Visually it didn't change volume, but became porous that

Experimental geoecology

confirmed reduction of samples mass. Therefore before preparation of the polished samples for SEM, material was impregnated with epoxy under vacuum for the purpose of giving of strength to it. According to EPMA the composition of crystal phase didn't change after leaching experiments, but "illumination" from glass disappeared (tab. 1). It is visible on the SEM-image in backscattered electrons of a cut cross to an axis of crystals that glass was completely leached (fig. 3b). Its place in samples for SEM was

taken by the hardened epoxy (black on the image). The area of crystals measured on a cut of 3x4 mm in size, cross to their extension, made 40%. This value can be transferred to a volume phases ratio – glass:crystals \approx 60:40 vol. %. Therefore, all glass from samples could be leached after the first three cycles of tests. After 7 days slower leaching of steadier crystal component of the material began, that explains the step of leaching rates at this boundary.

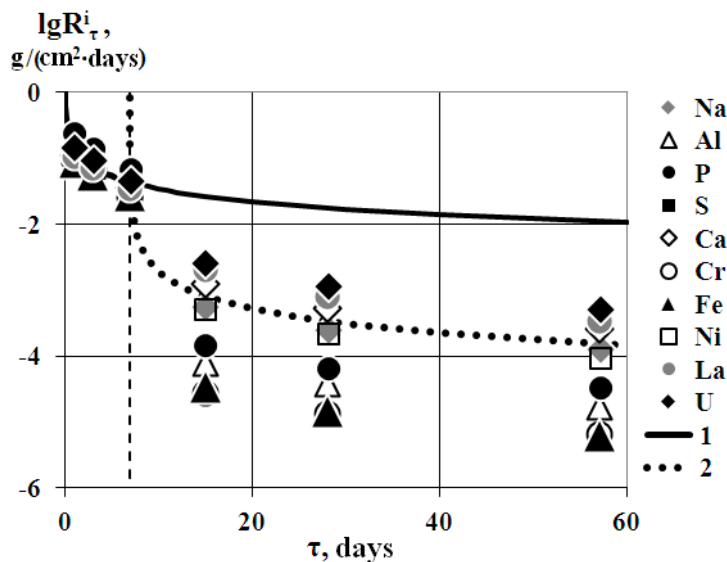


Fig. 5. Experimental data (symbols) and calculated curves of integrated leaching rates of glass (1) and crystal phase (2).

From the made supervision about phases ratio in initial material and assumptions of full leaching of glass after 7 days of experiments were defined dependences of integrated leaching rates on process duration for each of phases separately: $R_{\tau}^{gl}=0.155/\tau^{0.655}$ for glass and $R_{\tau}^{cr}=0.0052/\tau^{0.9}$ g/(cm²·days) for crystal phase (fig. 5). Differential rates of leaching on which compare matrixes according to the GOST state standard R52126-2003, can be calculated by means of the equations $R_n^{gl}=0.0535/\tau^{0.655}$ and $R_n^{cr}=0.00052/\tau^{0.9}$ g/(cm²·days). Depth of glass leaching is calculated on the equation $L_{\tau}^{gl}=0.129 \cdot \tau^{0.345}$ cm. Its value makes 0.25 cm for $\tau=7$ days that confirms the assumption of full leaching of glass from the material during this time interval. If the glass phase wasn't completely settled during tests, after 100 days the differential rate of its leaching would make $2.62 \cdot 10^{-3}$ g/(cm²·days). It is absolutely unacceptable indicator for HLW matrix material. According to requirements of the GOST state standard R50926-96 the value of matrixes leaching rate shouldn't exceed the size of 10^{-6} - 10^{-7} g/(cm²·days) for different radionuclides. The problem becomes aggravated because simulators of radionuclides were redistributed in glass at partial crystallization of melt. The crystal phase started being leached after full dissolution of the glass which is carrying out a role of the chemical buffer. Differential leaching rate of crystal phase after 100

days from the beginning of process by calculation has to equal $8.8 \cdot 10^{-6}$ g/(cm²·days).

Thus, the conducted researches showed that at rather slow (200°C/hour) cooling of the phosphate melt with HLW simulators corresponding to procedural composition of the glass received in EP-500 ceramic furnace at PA "Mayak" glass-crystal material was formed. Process of solidification was followed by crystallization differentiation of melt components: Al, Cr, Fe concentrated in crystal phase, Ca, Ni, La, U collected in glass. The glass-crystal matrix was leached in two stages. At the first stage glass was leached with an integrated rate of $n \cdot 10^{-3}$ g/(cm²·days). Thus simulators of radionuclides passed in the leachant. At the second stage which started after a total disappearance of glass, the crystal phase was leached with rate of $n \cdot 10^{-6}$ g/(cm²·days). Leaching rate of glass, and together with it, of radionuclides simulators on three orders exceeded expected size because of strong reduction of Al₂O₃ content in glass as a result of partial crystallization of melt. To avoid emergence of the described negative effects in the course of melt cooling during vitrification of real HLW, it is necessary to change temperature condition of melt cooling, or procedural composition of phosphate melt, by addition in furnace mixture of components-modifiers complicating crystallization.

References:

1. Vashman A.A., Dyomin A.V., Krylova N.V. et al. 1997. Phosphate glasses with radioactive waste. M.: CSRIatominform. 172 p.
2. Polyakov A.S., Borisov G.B., Moiseenko N.I. et al. 1994. Operating experience of EP-500/1R ceramic furnace for vitrification of liquid high level waste. *Atomnaya energiya*. Vol. 76. No. 3. P. 183-188.
3. Gusarov V.V., Mikirticheva G. A., Shitova V. I. et al. Phase ratios in glass-forming system $\text{NaPO}_3\text{-Al}_2\text{O}_3$. 2002. *Glass physics and chemistry*. Vol. 28. No. 5. P. 440-450.
4. Martynov K.V., Konstantinova L.I., Konevnik Yu.V., Zakharova E.V. 2014. Simulation of aluminophosphate glass leaching by underground waters after their interaction with clay engineering barriers. *Radiation safety problems*. No. 2. P. 43-50.

Martynov¹ K.V., Akhmedjanova² G.M., Nekrasov² A.N., Kotelnikov² A.R. Synthesis and studying of La-containing langbeinite-type zirconium phosphates under hydrothermal conditions

¹A.N. Frumkin Institute of Physical Chemistry and Electrochemistry RAS, Moscow

²Institute of Experimental Mineralogy RAS, Chernogolovka Moscow district

Abstract. The zirconium phosphates of langbeinite structural type: $(^{XII}MI)(^{IX}M2)_3\{(^{VI}LI)(^{VI}L2)(^{IV}PO_4)_3\}$, cubic cell, space group $P2_13$, $Z=4$, containing alkaline metals (Me=Na, K, Cs) and La as charge-compensating cations, were synthesized under hydrothermal conditions at a temperature 200°C and autoclave pressure of 1.55 MPa. It was shown that La was distributed between frame (L) and extra frame (M) structural positions in the ratio 1:2/3. The distribution coefficients of the components between zirconium phosphate langbeinites and nitrate water solutions were defined. It was established that for couples of alkaline metals the distribution coefficients decrease among $Kd_{Na/Cs} \geq Kd_{Na/K} > Kd_{K/Cs} \geq 1$, and for Me/La couples – among $Kd_{Na/Cs} \geq Kd_{Na/K} > Kd_{K/Cs} \geq 1$. It corresponds to reduction of an effective ionic radii difference of the cationic couples.

Key words: zirconium phosphates, langbeinite structural type, isomorphic replacements, hydrothermal synthesis, cationic exchange, distribution coefficient.

Citation: Martynov, K.V., G.M. Akhmedjanova, A.N. Nekrasov, A.R. Kotelnikov. 2015. Synthesis and studying of La-containing langbeinite-type zirconium phosphates under hydrothermal conditions. *Experimental Geochemistry*. Vol. 3. No. 4. P. X-XX.

http://exp-geochem.ru/JPdf/2015/04/Martynov03_eng.pdf

Earlier we reported about results of synthesis and studying of kosnarite structural type zirconium phosphates, as potential matrix material for an immobilization of radionuclides [Martynov, 2014₁]. Other kind of structure within which complex orthophosphates can crystallize, is the structure of langbeinite. The mineral langbeinite relates to the

class of sulfates – $\text{K}_2\text{Mg}_2(\text{SO}_4)_3$ and crystallizes in a cubic system (sp. gr. $P2_13$, $Z=4$). Like kosnarite, the elements consisting of two LO_6 octahedra linked to three TO_4 tetrahedra by shared oxygen atoms form a basis of langbeinite structure. Groups $[L_2(TO_4)_3]^{n-}$ form three-dimensional framework having n - charge. At the same time, in contrast to kosnarite framework, in langbeinite the columns of LO_6 octahedra run not along 3-fold axis c , but along four nonintercepting directions parallel to the body diagonals of a cube (fig. 1). Other difference from kosnarite is existence in langbeinite framework of two alternating nonequivalent octahedral positions which occupy, usually, two different cations [Orlova, 2005].

Crystal-chemical formula of the langbeinite-type orthophosphates can be presented as



where ^{VI}L is octahedral coordinate cations with charge $n = +2 - +5$: Mg, Co, Ni, Al, Fe, Cr, Ti^{3+} , Rh, $\text{P}3\text{O}$, Ti^{4+} , Zr, Nb, etc. Cavities of a framework (voids) ^{XII}MI and $^{IX}M2$ can be partially vacant (\square) or are occupied with cations having charge $n = +1 - +3$, for example: Na, K, Cs, NH_4 , Sr, Ba, REE, etc. Isomorphic replacements in langbeinite structure are carried out generally by the same principle, as in kosnarites [Martynov, 2014₂], but is also differences. The framework of langbeinite, as a rule, has a bigger charge, than a framework of kosnarite. "Norms" for these structures are framework charges equal -2 and -1 respectively. As a result of isomorphic replacements of framework forming cations they can decrease up to -1 and 0, or increase to -4 and -3. This fact defines fuller filling of extra frame positions in langbeinite, which also two, like in kosnarite. Absence or a small amount of vacancies in langbeinite dictates more limited terms for isomorphic replacements. There is obligatory an observance of a difference between framework forming and extra frame cations effective ionic radii in the range of 0.56-1.11 Å for preservation of structure [Orlova, 2011]. The sizes of langbeinite structure voids are more, than ones of kosnarite. It correlates with higher coordination numbers of cations in MI and $M2$ positions of langbeinite: 12 and 9 respectively. Therefore, larger cations, for example cesium or REE can easier occupy them formally. However, the windows dividing structural voids in langbeinite are much less, than in kosnarite. It explains lower conductivity of phosphates of monovalent elements with langbeinite structure in comparison with the compositions of NaSiCon-type having kosnarite structure [Isasi, 2000].

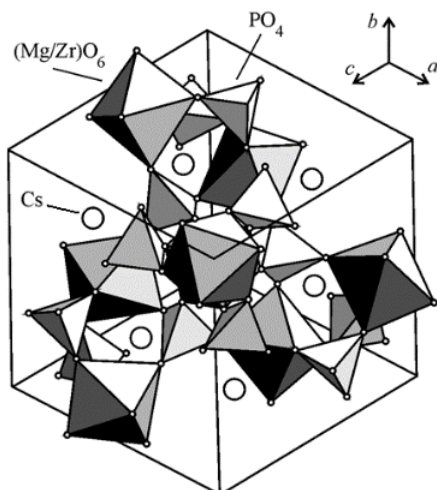


Fig. 1. Fragment of the $Cs_2Mg_{0.5}Zr_{1.5}(PO_4)_3$ structure having langbeinite type of crystal cell by data [Orlova, 2005].

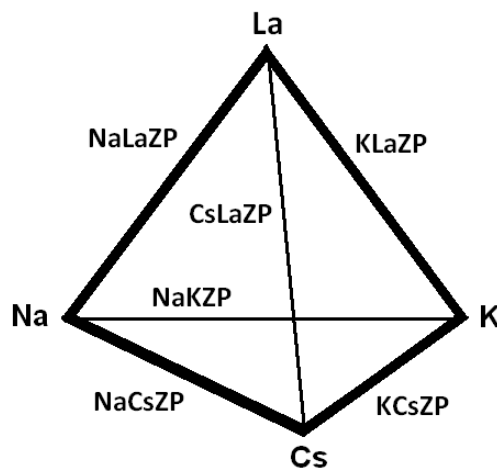


Fig. 2. Experimentally studied (fat lines) and calculated (thin lines) sections of the Na-K-Cs-La-zirconium phosphates.

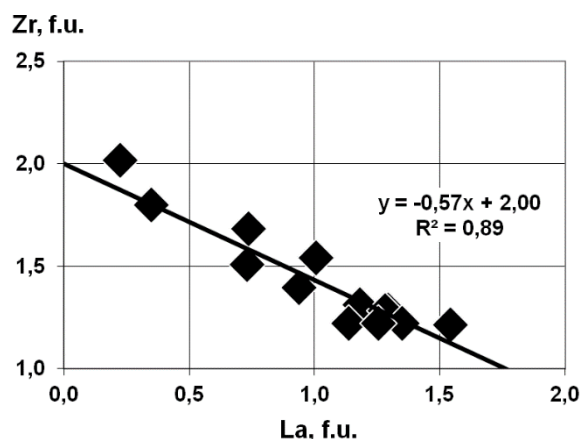
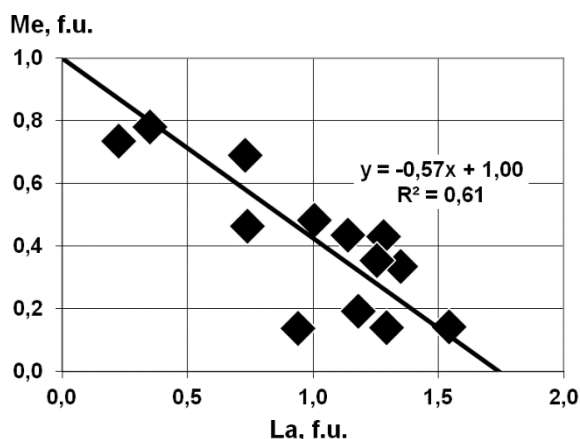


Fig. 3. The contents of the elements in synthesized (Na,K)-La-zirconium phosphate langbeinites by results of EPMA (SEM Tescan Vega II XMU with X-ray energy dispersive spectrometer Oxford Instruments INCAx-sight); f.u. – formula units.

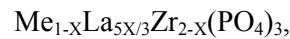
Theoretically noted specific features of langbeinite structure have to limit for its carriers ability to isomorphous replacements, especially by means of a cationic exchange. The purpose of our work consisted in experimental check how these limitations are essential, and in what measure it is possible to use isomorphism of zirconium phosphates having langbeinite structure to immobilize of radionuclides. For this purpose langbeinite-type zirconium phosphates containing alkaline metals (Me=Na, K, Cs) and La as framework charge-compensating cations were synthesized by hydrothermal method, and distribution coefficients of components between crystal phases and nitrate water solutions were defined. Hydrothermal experiments were made at a temperature 200°C under autoclave pressure of 1.55 MPa. Synthesis techniques of langbeinite zirconium phosphates, studying of cationic exchange equilibrium (distribution of components) between solid phases and water solutions, and researches of experimental products were similar to those which we used for studying kosnarite [Martynov, 2014₁]. Difference by

preparation of starting xerogels was that sols were neutralized by 25% ammoniac water to value pH=7-8 before evaporation. In cationic exchange experiments the mixes of 1 mol/l of alkaline metals nitrate solutions and 0.33 mol/l of $La(NO_3)_3$ solution were used. The contents of elements in quenching solutions after experiments were determined by methods of inductively coupled plasma mass spectrometry (Perkin Elmer Elan-6100) and inductively coupled plasma emission spectrometry (Perkin-Elmer Optima-4300 DV), and also the contents of alkaline metals – by emission spectrometry with flame atomization technique (KORTEC KVANT-2A).

Distribution of components has been studied in regional binary sections of four-component Na-K-Cs-La system (fig. 2). In the text and in figures the sections and the solid solutions corresponding to them are designated by symbols where the first two chemical elements mean couple of extra frame cations. For isoivalent sections interphase distribution of cations is described similar to an exchange of water solutions with kosnarite [Martynov, 2014₁].

Abstracts

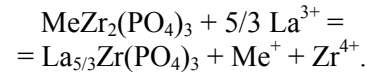
For heterovalent Me/La sections the cationic exchange of extra frame components is supplemented with replacement of part of Zr with La in *L* framework position. To understand how lanthanum, which takes *M* position in common with alkaline cations, and *L* position – together with Zr, is distributed between structural positions, it is necessary to analyze a ratio of contents of these elements in synthesized langbeinite (fig. 3). The limit content of La is close to 1²/₃ f.u. Thus there is a replacement within 1 f.u. Na and 1 f.u. Zr. Continuous change of La content as well as contents of Na and Zr replaced by La, testifies to the disorder nature of distribution of cations (La/Me, La/Zr) within one position. Such ratio of cations which is formed thanks to replacement is well described by binary solid solution



where $X=0-1$, and sum of reactions of a cationic exchange and replacement:



or in terms of chemical reactions:



Mole fraction of La in the solid phase (X_{ss}) and water solution (X_{fl}) are expressed as

$$X_{ss/fl} = 3 \cdot [\text{La}] / (3 \cdot [\text{La}] + 5 \cdot [\text{Me}]),$$

where $[\text{La}]$ and $[\text{Me}]$ is atomic concentration of La and alkaline metal in the corresponding phase. Coefficients of interphase distribution are defined as follows

$$\text{Kd} = [X_{ss} \cdot (1 - X_{fl})] / [(1 - X_{ss}) \cdot (X_{fl})^{5/3}].$$

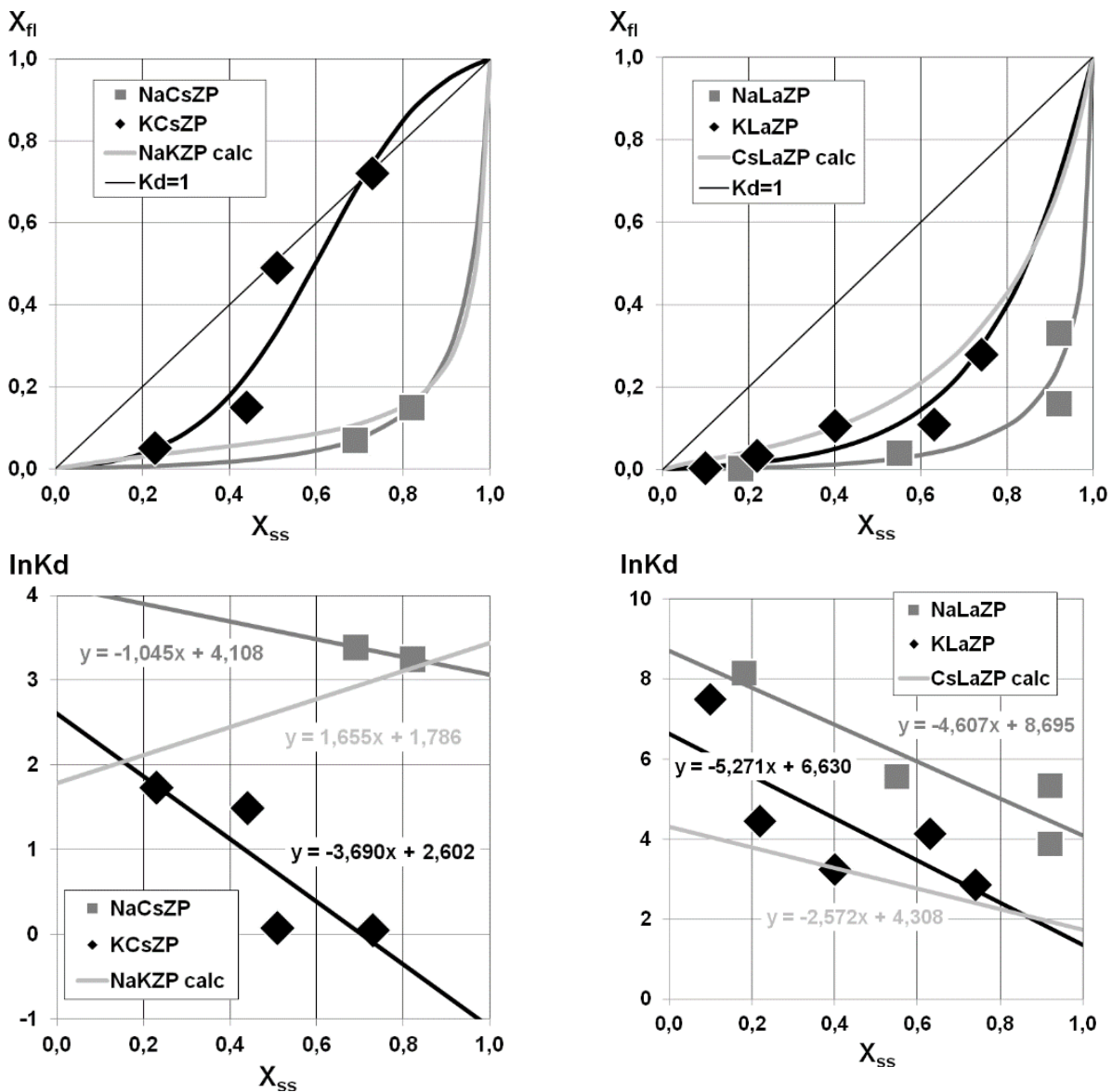


Fig. 4. The diagrams of interphase distribution (above) and dependences of $\ln Kd$ from solid solution composition (below) for distribution of elements between langbeinite-type zirconium phosphates and 0.33-1M nitrate water solutions at a temperature 200°C. Symbols – experimental data, lines – approximating and calculated curves.

Experimental geoecology

Experimental data were obtained for two isovalent (NaCsZP and KCsZP) and two heterovalent (NaLaZP and KLaZP) sections (fig. 4). The method of the analysis of $\ln K_d$ dependence on compositions of the coexisting phases described in [Martynov, 2014₁] was applied to processing of experimental data. For calculation of thermodynamic parameters of mixture of solid solutions next ratios were used:

$$\Delta G^0 = -R \cdot T \cdot (2 C_0 + C_1)/2 \text{ и } W = R \cdot T \cdot C_1/2,$$

where C_0 and C_1 are polynom coefficients

$$\ln K_d = C_0 + C_1 \cdot X,$$

W is mixture model parameter, ΔG^0 is Gibbs free energy (isothermal-isobaric potential) of the corresponding reaction, R is universal gas constant, T is temperature in K. For complex heterovalent reactions in Me/La couples combining exchange and replacement, parameter ΔG^0 has formal character because record of the equation of the sum of these reactions is formalized in itself. Its values are given

for understanding of the direction of shift of the resultant equilibria describing interphase distribution of components. Coefficients of the polynoms describing dependences of $\ln K_d$ on composition of solid phases were determined from experimental data by a method of linear regression. Values of the found thermodynamic parameters are presented in tab. 1, and the curves approximating experimental data – in fig. 4. Thermodynamic parameters for the sections which weren't studied experimentally (NaKZP and CsLaZP), were calculated proceeding from ratios:

$$\begin{aligned} \ln K_{d_{\text{NaKZP}}} &= \ln K_{d_{\text{NaCsZP}}} - \ln K_{d_{\text{KCsZP}}}, \\ \ln K_{d_{\text{NaLaZP}}} &= \ln K_{d_{\text{NaCsZP}}} - \ln K_{d_{\text{KLaZP}}}, \\ \ln K_{d_{\text{CsLaZP}}} &= \ln K_{d_{\text{NaLaZP}}} - \ln K_{d_{\text{NaCsZP}}}, \\ \ln K_{d_{\text{CsLaZP}}} &= \ln K_{d_{\text{KLaZP}}} - \ln K_{d_{\text{KCsZP}}}. \end{aligned}$$

The values received on each couple of the equations were average. Results of these calculations are also given in tab. 1, and calculated curves of cationic interphase distribution and dependences of $\ln K_d$ on langbeinite compositions are shown in fig. 4.

Table 1. Calculated sizes of Gibbs free energy of exchange and replacement reactions and energy of mixture model parameters for langbeinite-type zirconium phosphate solid solutions at a temperature 200°C. * – the sections studied experimentally

Sections	NaCsZP*	KCsZP*	NaKZP	NaLaZP*	KLaZP*	CsLaZP
ΔG^0 , kJ/mol	-14.11	-2.98	-10.28	-25.14	-15.71	-11.89
W , kJ/mol	-2.06	-7.26	3.26	-9.06	-10.37	-5.06

Two conclusions follow from the analysis of the calculated thermodynamic parameters (tab. 1). First, negative values of sizes ΔG^0 testify about shift of equilibria in all binary sections of the studied system towards enrichment of a solid phase by heavier cation in comparison with water solution ($K_d > 1$). Secondly, judging by mixture model parameters, all solid solutions, except NaKZP, have a negative deviation from ideality. It shows their high resistance to disintegration and phase transitions. Solid solution NaKZP, despite a positive deviation from ideality, also keeps negative values of free energy of mixture and stability in all range of compositions at a temperature 200°C. Our experiments showed that, despite the features of langbeinite structure, limiting ability to isomorphic replacements for its carriers, in practice even at heterovalent replacements in the zirconium phosphates, basic obstacles wasn't observed. It is probable this results from the fact that such replacements resulted not from a cationic exchange, and as a result of the recrystallization of solid phases which was followed by redistribution of cations between frame and extra frame positions. More strongly determined structure of langbeinite zirconium phosphates leads to that is more obvious for them, than for kosnarite analogs, communications

of K_d sizes with crystal-chemical parameters, in particular, with a difference of effective ionic radii of cations in exchange couples are expressed. Sequences of K_d decrease for couples of alkaline metals – $K_{d_{\text{Na/Cs}}} \geq K_{d_{\text{Na/K}}} > K_{d_{\text{K/Cs}}} \geq 1$, and for Me/La couples – $K_{d_{\text{Na/La}}} > K_{d_{\text{K/La}}} \geq K_{d_{\text{Cs/La}}} > 1$, strictly correspond to reduction of this difference.

As it was supposed on the basis of the sizes of extra frame voids, langbeinite zirconium phosphates have tendency to extraction of large cations from water solutions. These cations are Cs^+ and La^{3+} in the case under consideration. This property can be used for selective extraction of these nuclides against Na. As characteristic of extraction degree, the partition coefficient (α) is used usually. It is equal to the relation of distribution coefficients in two unicomponent systems containing N and M elements:

$$\alpha^{N/M} = [N_{ss}]/[N_{fl}] \times [M_{fl}]/[M_{ss}].$$

For two-component system containing isovalent cations (alkaline metals) this ratio can be written down in a look:

$$\alpha^{\text{Me2/Me1}} = X_{ss}^{\text{Me2}}/X_{fl}^{\text{Me2}} \times (1 - X_{fl}^{\text{Me2}})/(1 - X_{ss}^{\text{Me2}}) = K_d.$$

For a heterovalent cationic exchange integrated with replacement in Me/La couples it will be transformed to the following:

$$\begin{aligned} \alpha^{\text{La}^{3+}/\text{Me}^+} &= X_{ss}^{\text{La}}/X_{fl}^{\text{La}} \times (1 - X_{fl}^{\text{La}})/(1 - X_{ss}^{\text{La}}) = \\ &= K_d \times (X_{fl}^{\text{La}})^{2/3}. \end{aligned}$$

According to these ratios and the received experimental results langbeinite zirconium phosphates can take Cs from Na-Cs water solutions in the range of compositions $X_{\text{Cs}}^{\text{Cs}}=0.02-0.04$ in the solid phase having $X_{\text{ss}}^{\text{Cs}}=0.4-0.6$ with partition coefficient $\alpha^{\text{Cs/Na}}=40-32$, and La – from Na-La water solutions in the range of compositions $X_{\text{La}}^{\text{La}}=0.01-0.03$ in the solid phase having $X_{\text{ss}}^{\text{La}}=0.4-0.6$ with partition coefficient $\alpha^{\text{La/Na}}=52-41$. Such partition coefficients and contents of the taken elements in sorbents are insufficient for effective chemical technology of partition, but are quite acceptable for taking out radionuclides for the purpose of their immobilization in crystal matrix materials.

Thus, the received results showed that langbeinite-type zirconium phosphates can be used for taking out HLW elements, especially large cations, from water solutions, and their immobilization in the form of isomorphic components of a crystal matrix.

References:

1. Martynov K.V., Akhmedjanova G.M., Kotelnikov A.R., Tananaev I.G., Myasoedov B.F. 20141. Influence of replacement of phosphorus with silicon in kosnarite on its crystal-chemical and cationic exchange properties. *Experimental Geochemistry*. Vol. 2. No. 4. P. 460-465.
2. http://exp-geochem.ru/JPdf/2014/04/Martynov01_eng.pdf
3. Orlova A. I., Orlova V. A., Beskrovnyi A. I. et al. 2005. Synthesis and structural study of phosphates $\text{K}_2\text{Mg}_0.5\text{Zr}_1.5(\text{PO}_4)_3$, $\text{Rb}_2\text{Mg}_0.5\text{Zr}_1.5(\text{PO}_4)_3$, $\text{Cs}_2\text{Mg}_0.5\text{Zr}_1.5(\text{PO}_4)_3$ with langbeinite structure. *Crystallography Reports*. Vol. 50. No. 5. P. 759–765.
4. Martynov K.V., Lapitskaya T.S., Tananaev I.G. 20142. Influence of heterovalent replacements on crystal cell parameters and volume of kosnarite synthetic analogues. *Crystal chemistry, X-Ray Diffraction and Spectroscopy of Minerals – 2014*. Ekaterinburg: IGG UB RAS. P. 111-113.
5. Orlova A. I., Koryttseva A. K., Loginova E. E. 2011. A Family of Phosphates of Langbeinite Structure. *Crystal-Chemical Aspect of Radioactive Waste Immobilization*. Radiochemistry. Vol. 53. No. 1. P. 51–62.
6. Isasi J., Daidouh A. Synthesis, structure and conductivity study of new monovalent phosphates with the langbeinite structure. 2000. *Solid State Ionics*. Vol. 133. P. 303–313.

Razvorotneva¹ L.I., Vladimirov¹ A.G., Markovich¹ T.I., Gilinskaya¹ L.G., Grigorieva¹ T.N. The effect of mechanical activation on sorption properties of clay minerals

¹V.S. Sobolev Institute of Geology and Mineralogy SB RAS, Novosibirsk

Abstract. Effect of mechanical activation on the sorption capacity of layered silicates in respect of uranium was studied. There is an

increase in the specific surface area, crystal structure transformation, which leads to higher sorption uranyl ions. The formation of paramagnetic centers type O, $\text{O}_2^{\cdot-}$, OH^{\cdot} , Si-O involved in the binding of uranium were registered by EPR.

Key words: radionuclides, sorption, geochemical barriers, uranium.

Citation: Razvorotneva L.I., A.G. Vladimirov, T.I. Markovic, L.G. Gilinskaya, T.N. Grigoriev (2015). The effect of mechanical activation on the sorption properties of clay minerals. *Experimental Geochemistry*. T. 3. №.

http://exp-geochem.ru/JPdf/201X/XX/XXXXXX_rus.pdf

Strengthening the human impact on the ecosystem has led to increased interest in the techniques and methods used in radioecology. Thus, while developing methods for improving the environmental situation in areas of high accumulation of radioactive waste a tendency to establish geochemical barriers has begun to show. Principles of operation of such barriers are based on natural mechanisms of forming the accumulations of radioactive elements, with a clear emphasis on the study of the sorption properties of minerals [Kovalev, 1996]. In connection with this the search for cheap and fairly efficient sorption materials for binding and long-term retention of radionuclides is relevant and promising task. Uranium compounds are among the most toxic pollutants released into the environment as a result of the activities of the nuclear fuel cycle. For the purification of industrial process and waste waters from soluble forms of uranium clay minerals and peat are having prospects as natural sorption materials [Razvorotneva, 2007]. The parameters affecting the sorption performance of natural minerals, alongside with the pH, ionic strength, radionuclide concentration in a solution, also include the dimension of the sorbent particles, its specific surface area, pore size (micro, meso and macropores) and structural defects.

Sorption capacity of the clay minerals was determined by the change of the uranium concentration in the liquid phase after magnetic stirring for 2 hours. The ratio of solid and liquid phases was 1÷100. For sorption experiments a salt solution of uranium $\text{UO}_2(\text{NO}_3)_2 \cdot 6\text{H}_2\text{O}$ at a concentration of 25 mg/l was prepared. The amount of uranium in the solution was determined by mass spectrometry with inductively coupled plasma (ISP-MS) of high resolution by FINNIGAN MAT (Germany) by using a standard solution 10090a977 by "Merk". The determination error is 1-5%. The phase composition of solid samples was controlled by X-ray diffraction method on a DRON-3 diffractometer. EPR researches were performed on a radiospectrometer «Kadiopan», $f_{\text{mod.}} = 100 \text{ kHz}$, $T = 293 \text{ }^\circ\text{C}$. Filming of infrared spectra was made on the two-beam spectrometer Specord 75 IR in the range of 400-4000 cm^{-1} with the pure KBr tablet in the comparison channel. Measurements of surface area and pore size were carried out on the equipment

Experimental geocology

ASAP-2400 ("Micromeritics", USA) by nitrogen adsorption at 77 °K.

The effect of the size of the surface on the sorption capacity is most clearly manifested in the mechanical grinding. It is known that the rate of the heterophase interaction between the solid surface and the components of the liquid phase is not proportional to the amount of substance, but to the surface area. While machining the reactivity of solid phase is changing and the distortion of its structure appears. In the process of mechanochemical activation (MCA) the energy quanta interacting with the solution, commensurate with the strength of chemical bonds or exceed it. Therefore, one of the way of elastic energy concentration is the formation of structural defects in the crystal structure. For this purpose the method of mechanical activation in the centrifugal planetary mills EI 2 * 150 for 5, 10, 20 and 30 minutes was used.

Mechanical activation is associated with the disordering of the layered structures in kaolinites and montmorillonites. Table 1 shows the rates of changes in the degree of crystallinity during the MCA of kaolinite at dehydrated and aqueous media. In the X-ray structural analysis Hinckley index is a sensitive indicator of the degree of disorder in the layerwise space of clay minerals. The more ordered the structure is, the higher the value of Hinckley index. MCA in the dehydrated environment contribute significant changing in the structural indicators. In aqueous conditions, at neutral pH, and also in an acidic environment at pH 2.3 disordering of the structure occurs slightly.

Table 1. The effect of mechanochemical activation on the rates of crystallinity indices of kaolinite in dehydrated and aqueous media at different pH

Terms of mechanical activation		Crystallinity index	Sorption of uranium, %
Environment	pH		
Without activation	---	1.35	54.3
In water	2.3	1.31	56.9
In water	6.8	1.34	58.4
In water	9.2	1.08	67.2
Dehydrated	---	0.54	98.1

In the example of the kaolinite and montmorillonite (Table 2) it is showed that the amount of radionuclide retained on sorption clay barriers depends on the specific surface area and the degree of defectiveness of the near-surface layer. It was found that the high sorption capacity of kaolinites from individual fields is conditioned by structural abnormalities of various types, contributing to increasing of sorption capacities of clays.

Hydroxylated group ($\equiv \text{Si-OH}$ and $=\text{Al-OH}$), located on the edges of the crystal structure of clay minerals can bind significant amounts of uranium. The sorption at such sectors is strongly dependent on solution pH. Such dependence on the pH shows that the protons (H^+) located on the sorption surfaces, compete with uranium ions (U(VI)). Thus, at low pH values proton appears to be major sorbate agent that form a positive surfaces. With increasing pH uranium ions displace the H^+ and chemically interact with the hydroxyl groups on the surface.

Table 2. Physical and chemical properties of mechanochemical activated clay minerals

Mineral	Activation time, min	$I_{\text{rel.}}$	$S_{\text{spec.}}, \text{m}^2/\text{g}$	Hydroxyl groups, mEq/g	
				$\equiv \text{Si-OH}$	$=\text{Al-OH}$
Kaolinite	-	.	15.8	20	14
	10	0.53	41.3	350	240
	20	0.28	54.9	450	320
	45	0	47.2	700	450
Montmorillonite	-	1	64.3	100	80
	10	0.39	81.4	370	400
	20	0.13	88.2	640	500
	45	0	47.8	1250	930

In the IR spectra at dehydrated MCA the intensity of the bands of stretching vibrations of surface OH groups reduces: the maximum 3688 cm^{-1} disappears, but the band 1630 cm^{-1} appears. This band corresponds to the deformation vibrations of water formed by the condensation of surface -OH groups. With increasing of time of MCA influence along with deformation of structural layers and dehydration of the surface layer of kaolinite the separation of proton from the OH group occurs. The

appearance of protons is captured by the change in intensity of the absorption bands of stretching vibrations of -OH groups in the area 1700 cm^{-1} .

Judging by the nature of changing in the parameters of fine structure (reduction of the sizes of coherent-scattering regions (CSR) and microdeformations) during 10 minutes of mechanical activation meso- and micro-defects are formed (Table 3), that leads to an increase in capture of implanted ions UO_2^{2+} .

Abstracts

Table 3. Properties of disordering in structure of kaolinite subjected by mechanical activation

Activation time, min	CSR, Å	$\sqrt{\varepsilon^2}$
Original sample	580	0.07
Activating in the air, 1 min	210	0.40
Activating in water, 1 min	510	0.08

$\sqrt{\varepsilon^2}$ - absolute rms microdistortions

As result of the fact that the number of distortions in the structure of clay minerals increases along with the decrease of particle size, uncompensated paramagnetic states occur, recorded by the EPR method. In the studied samples of clays Fe^{+3} ions in the octahedral positions are registered, as well as centers of O^- , O_2^{3-} , OH^0 , Si-O^- types. Besides structural centers in the samples of montmorillonites the ESR spectrum of impurity microphase of ions Fe^{+2} is recorded, which represents itself a wide (about 130 mT) line with $g = 2.05$. In natural samples of clay minerals the microphases of Fe^{+3} is almost always present, their EPR spectra are presented as broad lines (150 mT or more) in a large range of values of g - factors. The experiments on the uranyl sorption proved the effectiveness of the participation of these phases of iron.

The emphasis is placed on the following experimental facts:

a) after the uranyl ion sorption the intensity of EPR centers decreases about 2 times, and in some samples, they disappear completely;

b) in the montmorillonites with sorbed UO_2^{2+} in the EPR spectrum the wide (80-120 mT) symmetric line of Fe^{+3} complexes in $g = 2.00$ appears, that indicates the redox interaction of U (VI) with an impurity of Fe^{+2} included to the structure of the clay mineral;

c) during annealing of paramagnetic centers conducted in the temperature range of 100 – 650 °C, clay sorption capacity decreases by 30-50%, which indicates that the absorbent activity of the clays is not only connected with ion exchange processes, but also with unsaturated valence states on the surface (Table 4).

Table 4. The changing the sorption rates of clay minerals with increasing annealing temperature

Montmorillonite		Kaolinite	
T °C	Sorption of uranium, %	T °C	Sorption of uranium, %
0	100	0	100
100	80	100	82
200	79	150	82
250	84	250	65
350	89	350	69
450	50	450	60
550	10	550	39

The work was supported by the interdisciplinary integration project No. 110

References:

1. Kovalev V.P., Mel'gunov S.V., Puzankov Y.M. et al. 1996. Prevent uncontrolled spread of radionuclides into the environment (geochemical barriers on the basis of smectite). - Novosibirsk: Publishing House of SB RAS. 162 p.
2. Razvorotneva LI, Boguslavskiy AE, Kovalev VP et al. 2007 Sorption of uranium in geochemical barriers on the basis of peats of different genesis. *Ecology of industrial production*. №3. P. 33-37.

Khushvakhtova S.D., Tyutikov S.F., Danilova V.N., Ermakov V.V. Biogeochemical monitoring of the urban landscape

V.I. Vernadsky Institute of Geochemistry and Analytical Chemistry RAS, Moscow

Abstract. The biogeochemical assessment of the linden alley in Moscow by means of an integrated comparative study of soils, chemical composition and morphological parameters of leaf linden are presented. The most differences between the variants were marked by the degree of pathology leaves (chlorosis and necrosis) and the content of pigments (chlorophyll and carotene). The data obtained reflect the impact of the application of de-icing salts and automobile emissions.

Keywords: *Alley, biogeochemical monitoring, salinity, lime, minerals, anti-icing agents, pigments soil, phytochelatins.*

Citation: Khushvakhtova S.D., S.F. Tyutikov, V.N. Danilova, V.V. Ermakov. 2015. Biogeochemical monitoring of urban landscape. *Experimental Geochemistry*. V. 3. No. .

Introduction. Green areas in towns along the highways are often subject to severe stress due to heavy traffic of cars, the impact of toxic emissions and the use of de-icing agents (DIAs) in the cold season. Furthermore, the motor vehicle emissions and DIAs may have adverse ecological implications for urban environment because of soil and/or atmospheric precipitate salification. Unfortunately, methods for ecological state estimation of urban areas are inadequately developed, and it is equally applies to forest plantations laid out along urban highways. This equally applies to the areas of forest plantations along the city highways.

The goal is to carry out a multifactorial estimation of a linden parkway located in Kosygin Street in the western part of Moscow using a range of up-to-date techniques including the use of phytobiomarkers.

Material selection and methods. On the Vorobyovy Hills, linden leaf samples and soil samples from under these trees were collected in 10 points. Points 1, 3, 5, 7 and 9 were classified as conditionally “polluted” sites located on the right side of the parkway, and points 2, 4, 6, 8 and 10 were selected as relatively background ones (see Fig. 1).



Fig.1. Location diagram for sampling points in Kosygin Street.

The trees were of about the same age with the stem diameter ranging from 40 to 45 cm. We cut 50 linden leaves per a tree at average human height (e.g., about 1.8 to 2 m), in 10 points. Furthermore, at the sampling sites, chlorosis/necrosis levels were estimated using the following scoring: 1 – singular spots, 2 – up to 3 spots on the leaf, 3 – 4 to 5 spots, 4 – more than five and up to ten, 5 – mass necrosis. The scoring of the affected area ran as follows: 1 – isolated spots, 2 – spots covering up to 1 cm², 3 – more than 1 cm² and up to 2 cm², 4 – more than 2 cm² and up to 5 cm², and 5 – more than 5 cm², large sized spots or foci.

The average soil samples were delivered to the laboratory, weighed, and after drying and humidity level determination, soil lots (the fraction ≤ 1 mm) were taken to prepare soil extracts (the aqueous one and 1 M KCl) to be used for atomic absorption determination of metal levels, and for other purposes.

The humidity levels for linden leaves, the asymmetry factor (AF) and content of phytochelatin were determined. The alcoholic extracts were determined the chlorophylls "a", "b" and carotenoids in the alcoholic extracts were measured by means of spectrophotometry. Prepared extracts were used for derivatization the SH-compounds by N-9(acridinyl)maleimide (NAM) after reduction with sodium borohydride for determination of phytochelatin [Danilova et al., 2014]. Trace element levels in soil and linden leaf samples were determined in AAS using the assay flame and flameless versions, following the sample mineralization with a mixture of nitric and perchloric acids using devices "QUANT-Z.ETA" with Zeeman background correction, or "QUANT-2A". In the 1 M KCl extract, pH was measured, and in the aqueous extract, cations (Ca²⁺, Mg²⁺, K⁺, Na⁺, NH₄⁺) and anions (Cl⁻, SO₄²⁻) were measured. Also, water-soluble phosphates were determined photometrically, and mineralization extracts were determined using

conductometer COM 80, and also organic matter content levels in soils were determined in accordance with the method [GOST 26213-91].

Results

Macro components of soils. Almost all the soils studied were fill up urban soils periodically fertilized with turf and mineral amendments. The organic matter contents in soils varied respectively from 7.0 to 13.9% (background) and from 12.2 to 16.5 (parkway), and the pH indices from 6.0 to 7.0 (background) and from 6.7 to 6.9 (parkway). It was found a higher content of calcium, magnesium, sodium and potassium in the soil sampled within the alley. Furthermore, in the "polluted" soils collected at the beginning of the route (see points 1 and 3), the above macro element concentrations were higher as compared with the points at the end of the route. This is apparently due to the chemical elements migration and accumulation as a result of the height difference (the hillside from point 10 to point 1 is implied). In addition, the accumulation of calcium, magnesium, sodium and, to a lesser extent, potassium is associated with the use of de-icing agents that are transferred to the head of Kosygin Street with snowmelt waters because of a significant height difference making about 36 m. Besides, rain precipitations and water flows that promote the parkway cleansing play an important role here.

Also, relatively low lead concentrations in the soils which approximate to MRLs for metal levels in soil (e.i., 20 to 33 mg/kg) [Nikiforova et al., 2014] are noteworthy. Apparently, this is due to the fill-up nature of the urban soils, percolative regime of the linden parkway soils, and relatively low motor traffic observed up to the 1990s.

The data for water-soluble component levels in the soils are summarized in Table 1.

Abstracts

Table 1. Chemical composition of soil aqueous extracts expressed in centimols(eq) per 1 kg of soil

No. point	pH (KCl)	Ca ²⁺	Mg ²⁺	K ⁺	Na ⁺	Cl ⁻	SO ₄ ²⁻	NH ₄ ⁺	HCO ₃ ⁻	PO ₄ ³⁻	Σ ions	M*, mg/kg
Conditionally background areas												
2	6.0	0.101	0.09	0.38	1.17	0.82	0.44	0.06	0.26	0.009	3.26	670
4	6.4	0.055	0.08	0.08	0.96	0.72	0.13	0.05	0.32	0.002	2.27	570
6	6,6	0.401	0.09	0.08	0.87	0.70	0.21	0.06	0.35	0.001	2.70	500
8	7.1	0.303	0.09	0.26	0.78	0.64	0.23	0.07	0.42	0.003	3.42	500
10	6.5	0.204	0.09	0.36	0.85	0.82	0.21	0.02	0.34	0.025	2.89	420
Mean	6.52± 0.26	0.213± 0.111	0.088± 0.003	0.23± 0.12	0.93± 0.11	0.74± 0.22	0.24± 0.13	0.052± 0.014	0.34± 0.04	0.008± 0.007	3.16± 0.27	532± 70
Lots on lime avenue												
1	6.8	0.352	0.34	0.90	2.52	2.97	0.47	0.02	0.38	0.003	7.93	2030
3	6.8	0.254	0.09	0.36	2.35	2.67	0.14	0.02	0.38	0.001	6.22	680
5	6.8	0.503	0.17	0.36	1.01	1.34	0.16	0.01	0.38	0.003	3.92	420
7	6.9	0.501	0.09	0.15	2.17	1.31	0.60	0.07	0.40	0.002	5.22	670
9	6.7	0.451	0.17	0.10	0.95	0.82	0.42	0.02	0.36	0.004	3.17	320
Mean	6.80± 0.04	0.412± 0.087	0.172± 0.067	0.37± 0.21	1.80± 0.66	1.82± 0.80	0.36± 0.17	0.028± 0.017	0.38± 0.01	0.023± 0.007	5.29± 1.43	824± 482

* Mineralization content indices for extract (after the conductometer indications).

It is easy to notice that considerable amounts of salts are extracted with water. In the extracts prepared from conditionally polluted soils, the average content levels for the most of cations and anions are 1.2 to 2.5 times higher than their concentrations for extracts from conditionally background soils. The highest salt concentrations are found in soil extracts from point 1 at the beginning of the route (the total ionic content is 7.93 and the mineralization content is 2030 mg/kg) which is consistent with the soil macro composition. The obtained data suggest that it is the most contaminated area among the ones examined.

However, as compared with the data available for chemical composition of soils in Moscow, the soils

under test exhibit moderate contamination levels. The increased chloride content levels as observed for the linden parkway soils (namely, 1.82 ± 0.80 cmol(eq)/kg) are accompanied by densification of sodium and/or other cations indicating moderate salinity levels of the soil sites examined.

Trace element composition of soils and linden leaves

The trace element composition patterns of both soil and linden leaf samples collected at conditionally background points and sites located within the parkway vary insignificantly (see Table 2).

Table 2. Trace element content levels in soil and linden leaf samples expressed in mg/kg of the dry matter

Object	Cu	Pb	Mn	Fe	Cd	Zn	As	Ni	Mo	Cr	Sr
Conditionally background areas											
Soil	33.2± 21.6	29.4± 25.7	204± 43.2	9222± 2482	0.39± 0.39	104± 75.8	2.73± 1.90	3.53± 1.16	0.16± 0.03	1.91± 0.61	49.2± 32.8
Linden leaves	9.72± 1.94	1.74± 0.79	128.4± 103.7	351± 88.8	0.074± 0.061	16.2± 6.72	0.053± 0.019	0.42± 0.12	0.11± 0.05	0.11± 0.04	36.1± 23.7
Linden alley											
Soil	26.2± 11.1	22.3± 11.9	401± 150	11178± 2122	0.39± 0.13	76.8± 34.6	3.61± 1.77	3.84± 1.32	0.17± 0.03	1.58± 0.42	74.7± 72.8
Soil	26.2± 11.1	22.3± 11.9	401± 150	11178± 2122	0.39± 0.13	76.8± 34.6	3.61± 1.77	3.84± 1.32	0.17± 0.03	1.58± 0.42	74.7± 72.8

Nevertheless, there are some differences in manganese content levels; thus, in the conditionally background areas, manganese levels are 2 times as lower, but it has no significant effect upon linden leaves. The iron levels for the parkway linden leaves and soils are 2 times and 1.4 times higher,

respectively. In soils originating from man-made sites, higher strontium levels are observed, though the data scattering is significant.

Selenium content indices for soils of the background and conditionally polluted sites showed 1.6-fold difference: 441 ± 179 and 639 ± 212

Experimental geoecology

mcg/kg, respectively. Selenium average levels for leaves were 171 ± 45 and 152 ± 20 mcg/kg of the dry matter, and selenium biological absorption coefficient for linden leaves dropped within the linden parkway as follows: 0.42 ± 0.08 (for background) and 0.26 ± 0.06 (for conditionally polluted sites).

Morphological and biochemical parameters of linden leaf

On the average, humidity levels for linden leaves collected in background sites and those for the parkway were 61.4 ± 1.7 and $58.2 \pm 1.4\%$, respectively.

Linden leaves collected in the parkway were found to be less wet which seems to be associated with a stronger light intensity on the right side of the parkway. Also, the parkway leaves were not only drier but also had pronounced signs of necrosis and/or chlorosis. According to the scoring system applied, linden leaves taken from conditionally background and polluted sites differed drastically (4.6 ± 0.7 and 10.8 ± 5.4 , respectively). Moreover, the extent of injury leaves from some linden trees differed markedly, as evidenced by the arithmetic mean deviation high value (± 5.4). No differences in asymmetry of linden leaf right and left halves were determined. For the conditionally background sites, this parameter was equal to 1.138 ± 0.036 , and for the parkway 1.122 ± 0.018 .

The chlorophyll "a", chlorophyll "b" and carotin concentrations in the leaves taken from conditionally background sites are significantly higher as compared with pigment content levels for the parkway linden leaves, with the exception of the first two points. No correlation between this compounds and total metal (Pb, Zn, Cd, Cu) concentrations in linden leaves was revealed. Seemingly, the relatively low metal accumulation in leaves does not promote phytochelatin synthesis.

Conclusion. The multivariate monitoring carried out on one of the sites of the Vorobyovy Hills showed a relatively satisfactory condition of the linden parkway located in Kosygin Street. The salinity level of urban soils collected within the range of Kosygin Street was found to be moderate as compared with other areas of the city [Nikiforova et al., 2014], which was due to accumulation of chlorides of alkaline and alkaline-earth elements used as de-icing agents. No toxic concentrations of macro and micro elements were also found. Nevertheless, a number of plants in the linden parkway on the right side of the street are subject to detectable effect of intense solar radiation, which results in early leaf necrosis & chlorosis followed by its drying out. Apparently, irrigation and watering of the trees should be more copious. The pathological reactions of linden leaves have no significant effect on lamina

asymmetry pattern though being associated with a decrease in the synthesis of some pigments (like chlorophyll or carotenoids) and water metabolism imbalance (dropped humidity levels in leaves). As far as the test for phytochelatin is concerned, it was found ineffective here which is due to low levels of metals as accumulated in linden leaves. Apparently, the synthesis of thio-containing biologically active compounds is induced at higher metal concentrations in the cytosol of plant cells.

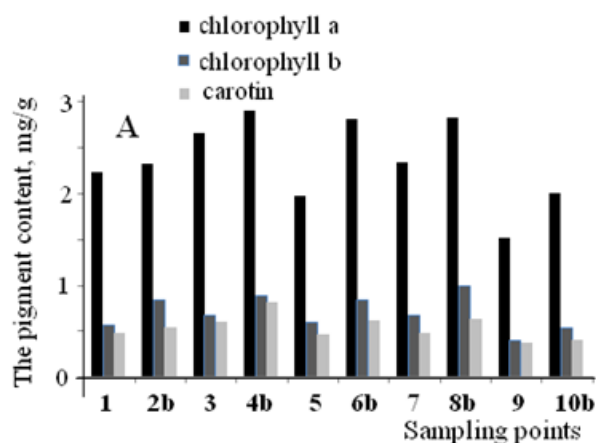


Fig. 2. Changes in the concentration of pigments in the leaves of linden in pilot sites; b - conditioned background.

Supported by RFBR grant № 15-05-00279/

References:

1. Danilova V.N., Khushvaktova S.D., Ermakov V.V. 2014. Application of HPLC-NAM spectrofluorometry to determine sulfur-containing compounds in biogeochemical objects. *Experimental Geochemistry*. Vol. 2. No. 4. P. 445-448.
2. Nikiforova E.M., Kosheleva N.G., Vlasov D.V. 2014. Monitoring of snow and soil salinization of the Eastern District of Moscow by means of icing mixtures. *Basic Research. Biological sciences*. No. 11. P. 340-347.
3. GOST 26213-91 Soils. Methods for the determination of the organic substance. M.: State Standard, 1993. 8 p.